Bioinspired urease-powered micromotor as an active oral drug delivery carrier in stomach

Hyunsik Choi, Sang Hoon Jeong, Tae Yeon Kim, Jeeyoon Yi, Sei Kwang Hahn[*]

Department of Materials Science and Engineering, Pohang University of Science and Technology (POSTECH), 77 Cheongam-ro, Nam-gu, Pohang, Gyeongbuk, 37673, South Korea

ARTICLE INFO

ABSTRACT

Self-propelling micro- and nano-motors (MNMs) have been extensively investigated as an emerging oral drug delivery carrier for gastrointestinal (GI) tract diseases. However, the propulsion of current MNMs reported so far is mostly based on the redox reaction of metals (such as Zn and Mg) with severe propulsion gas generation, remaining non-degradable residue in the GI tract. Here, we develop a bioinspired enzyme-powered biopolymer micromotor mimicking the mucin penetrating behavior of *Helicobacter pylori* in the stomach. It converts urea to ammonia and the subsequent increase of pH induces local gel-sol transition of the mucin layer facilitating the penetration into the stomach tissue layer. The successful fabrication of micromotors is confirmed by high-resolution transmission electron microscopy, electron energy loss spectroscopy, dynamic light scattering analysis, zeta-potential analysis. In acidic condition, the immobilized urease can efficiently converted urea to ammonia, comparable with that of neutral condition because of the increase of surrounding pH during propulsion. After administration into the stomach, the micromotors show enhanced penetration and prolonged retention in the stomach for 24 h. Furthermore, histological analysis shows that the micromotors are cleared within 3 days without causing any toxicity in the GI tract. The enhanced penetration and retention of the micromotors as an active oral delivery carrier in the stomach would be successfully harnessed for the treatment of various GI tract diseases.

1. Introduction

The mucus layer in the body covers all wet epithelial surfaces such as the airway system, the gastrointestinal (GI) tract and the urinary tract with several protection mechanisms from the invasion of pathogens [1, 2]. The viscous mucus layer prevents not only the penetration of microorganisms into the host tissues but also the delivery of therapeutic drugs [3]. Especially, the oral drug delivery in the stomach is highly limited by the harsh condition of very low pH and the barrier of mucus layer. Nevertheless, due to the great patient compliance, most of pharmaceuticals in the market are developed for oral delivery [4]. Accordingly, the development of oral delivery strategy for efficient drug uptake into the stomach would make a huge impact on the field of medical and pharmaceutical industries.

With the progress of nanotechnology, self-propelling micro- and nano-motors (MNMs) have emerged as an alternative to the traditional passive delivery systems. The MNMs enable greatly improved sensitivity

of biosensing and highly efficient drug delivery due to their superior characteristics including agitation effect, rapid transport, active targeting and high tissue penetration [5,6]. Recently, a number of MNMs have been developed for specific tissue targets such as GI tract [7–13], urinary tract [14], blood clot [15–17] and deep tumor tissues [18]. Especially, MNMs for oral delivery have attracted great attention for targeting GI tract [7–13]. Wang's group developed Zn or Mg based micromotors, propelled by the generation of hydrogen bubbles in the stomach. They showed the improved binding and retention behaviors in the stomach. However, the propulsion of micromotors by explosive and aggressive redox reaction of metals can cause tissue damage during penetrating into the stomach wall. Moreover, non-degradable residues in the stomach wall without clearance might cause unexpected immune response and potential toxicity. Fischer's group proposed magnetic field actuating microswimmer for *in vitro* mucin penetrating as a proof-of-concept study [19]. The enzyme-immobilized microswimmer could efficiently penetrate *in vitro* mucin gel by gel-sol transition of mucin gel. However, the

---

microswimmer is also composed of non-degradable metal composites (such as Ni, Al_2O_3) and, they did not show any *in vivo* mucin penetration and clearance test. Accordingly, effective *in vivo* mucus penetrating MNMs with biocompatible reaction and clearance are highly required for treating stomach diseases.

Here, we developed bioinspired urease-powered polydopamine (PDA) micromotor as a biomimetic system of *Helicobacter (H) pylori* for active oral drug delivery in the stomach. As reported elsewhere [20–23], our micromotor used urea in stomach as a bioavailable power source for the propulsion of synthetic motors. The micromotor was prepared with a PDA hollow microcapsule, which showed not only good biocompatibility and biodegradability but also muco-adhesive property [24–27]. Just like the mucin penetrating *H. Pylori* [28,29], urease conjugated micromotor catalyzed the hydrolysis of urea to release ammonia and the subsequent local pH increase induced the gel-sol transition of the mucus layer, enabling the facile penetration into the stomach wall with propulsion (Fig. 1). In acidic condition, the immobilized urease could efficiently converted urea to ammonia, comparable with that of neutral condition because of the increase of surrounding pH during propulsion, demonstrating feasibility of micromotors for *in vivo* stomach applications. After oral administration of micromotors into mice, the micromotors were assessed for the enhanced penetration to the stomach wall and prolonged retention in the stomach. In addition, after 3 days, the histological analysis was carried out to confirm the safety and the total clearance of micromotors from the stomach. To our best knowledge, this is the first report on an enzymatically propelled micromotor for *in vivo* muco-penetration in the stomach.

2. Materials and methods

Materials. Silica microparticle, urease from Canavalia ensiformis (type IX, powder, 50,000–100,000 units per g of solid), mucin,
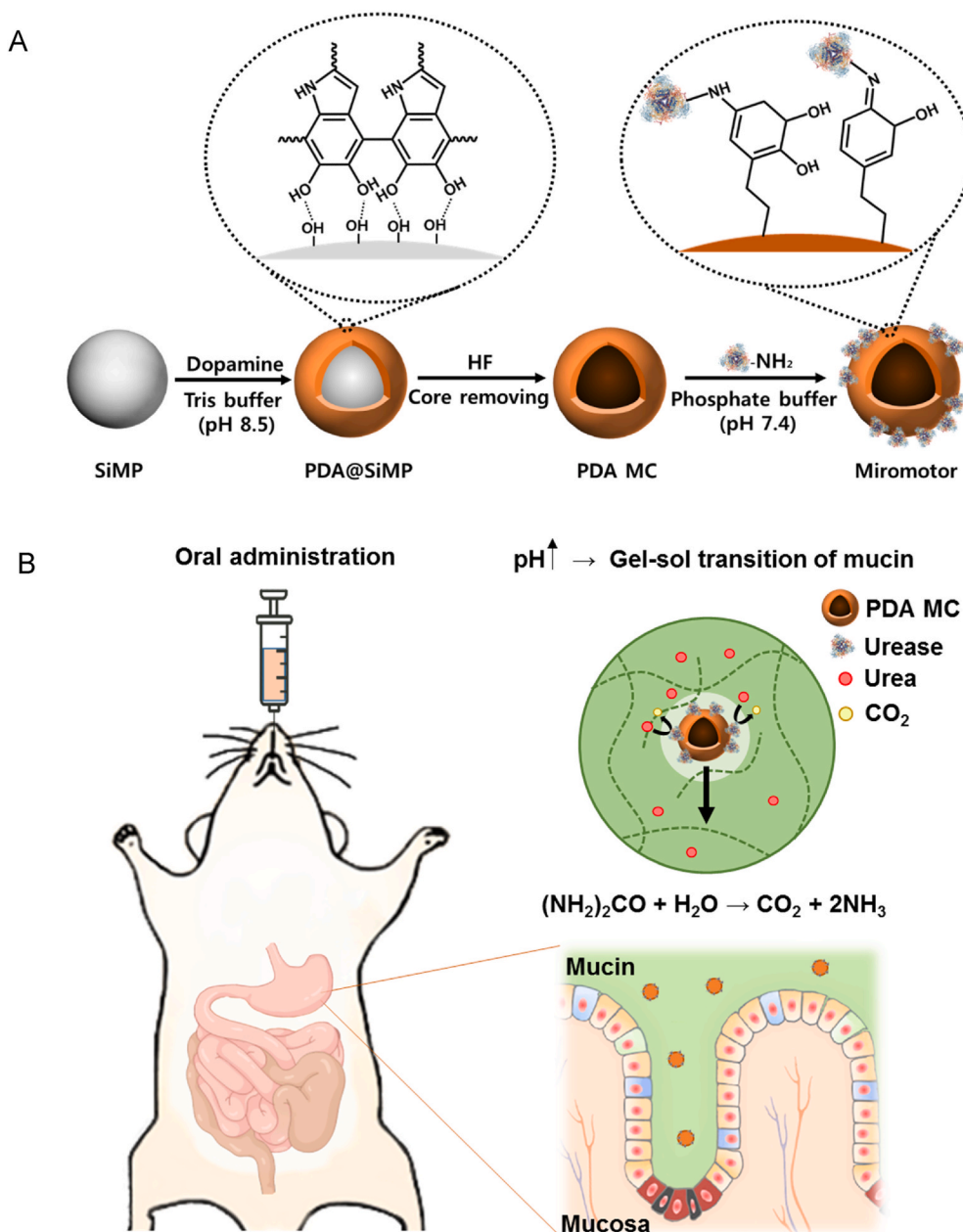
Fig. 1. Schematic illustration for (A) the preparation procedure of urease-powered micromotors using silica microparticle (SiMP) and polydopamine microcapsule (PDA MC), and (B) the oral delivery of urease-powered polydopamine micromotors for enhanced penetration and retention in the stomach.

hydrofluoride (HF), ammonium fluoride (NH4F), dopamine hydrochloride, phosphate buffered saline (PBS), tris(hydroxymethyl)aminomethane, fluorescein isothiocyanate (FITC), 3-aminopropyltriethoxysilane (APTES), urease activity assay kit were purchased from Sigma Aldrich (St. Louis, MO). One unit of urease is the amount of enzyme that catalyzes the formation of 1.0 μmole ammonia per minute at pH 7.0. BCA protein assay kit was purchased from Thermo Fisher Scientific (Waltham, MA).

Preparation of polydopamine microcapsule. Polydopamine microcapsule (PDA MC) was synthesized as previously reported elsewhere [30]. In brief, 10 mg of silica particles (5 wt%) were prewashed 3 times with 10 mM TRIS buffer (pH 8.5). The resulting pellet was resuspended in 2 mL of a dopamine hydrochloride solution (2 mg/mL) in 10 mM TRIS buffer. The suspension was darkened within 10 min and the reaction was proceeded for 12 h with constant shaking. After that, the tan-colored particles were centrifuged (1000 g, 30 s) and washed with fresh TRIS buffer thrice to remove the excess dopamine. PDA MC was formed by removing the template silica core with 2 M HF/8 M NH4F mixed solution (pH 5) at 20 °C for 5 min, followed by 3 cycles of centrifugation/redispersion process (8000 rpm for 5 min).

Preparation of micromotor. PDA MC was dispersed in PBS containing urease (5 mg/mL). The reaction was proceeded with constant shaking at room temperature for 12 h. After that, the urease functionalized polydopamine micromotor solution was washed with PBS three times by centrifugation (4500 g for 5 min) and dispersion with sonication for 3 min.

Characterization of micromotor. The size and characteristic morphology of micromotors were analyzed by electron energy loss spectroscopy (EELS) equipped high resolution - transmission electron microscopy (HR-TEM, JEM-2200FS, JEOL, Japan) at 200 kV. Five μL of nanodroplets (5 mg/mL) was deposited onto a copper grid. The grid was dried in a desiccator for 5 days and then observed by HR-TEM. In addition, the hydrodynamic size and surface charge of the samples were analyzed with a dynamic light scattering instrument (DLS, Zetasizer Nano-ZS, UK) at room temperature. The micromotors in each fabrication step were analyzed by Fourier transform - infrared spectroscopy (FT-IR, Varian 620-IR, Agilent, Santa Clara, CA).

Immobilized urease activity test. The concentration of urease immobilized onto the micromotor was measured by using the BCA protein assay kit. The urease activity according to pH was measured with a commercial urease activity assay kit. Ninety μL of micromotor (5 mg/mL) solution was added to the 10 μL of urea. After incubation for 10 min, the activity was measured by the colorimetric method (absorbance at 670 nm). The change of pH is monitored with a pH meter (FP20, METTLER TOLEDO, Columbus, OH).

Motion analysis of micromotors. The movement of micromotors were recorded using an inverted microscope with a frame rate of 35 fps. The micromotor sample solutions were mixed well with the urea containing solution (0, 5, 10, 20 mM). In addition, the movement was also analyzed in acidic condition and gastric fluid (containing 2 mg/mL of NaCl at pH 3). The MSD was calculated by using 20 nanomotors for each condition. The diffusion coefficient and the velocity of micromotors were determined by fitting the MSD data to the following equation, respectively:

$$MSD(\Delta t) = 4 \times D_e \times \Delta t \ (linear \ increase)$$

$$MSD(\Delta t) = (v \times \Delta t)^2 + 4 \times D_e \times \Delta t \ (non-linear \ increase)$$

Rheological analysis of mucin gel. The rheology of mucin gel was analyzed by using a rheometer (MCR 92, Anton Paar, Torrance, CA) with a 25 mm size plate. The loss modulus and storage modulus were mesured from 0.1 to 10 rad/s of frequency with 1% strain.

Tagging with FITC. To label PDA MC and micromotors with FITC, 100 μL of FITC solution in PBS (0.1 mg/mL) was added to 2 mL of PDA MC and micromotors solutions, respectively. The mixtures were incubated at room temperature with shaking in the dark for 2 h. The

resulting solutions were centrifuged at 8000 rpm for 5 min to remove excess FITC molecules. As a control, FITC was also functionalized onto the surface of silica microparticles as previously reported elsewhere [31]. Fifty μL of aminopropyl triethoxysilane (APTES) was added into the silica microparticle solution (2 mL, 5 mg/mL in ethanol) to introduce amine groups onto the surface of silica microparticle. After stirring at room temperature for 12 h, modified silica microparticles were centrifuged (1000 g, 30 s, 3 cycles) to remove the excess APTES. After that, 1 mL of the amine-modified silica microparticle solution was mixed with 500 μL of FITC solution in ethanol. After stirring for 4 h, the particles were collected by centrifugation/redispersion processes (1000 g, 30 s, 3 cycles). Fluorescence intensity was measured with a spectrofluorometer (FL-1039, Horiba Scientific Co., Japan).

Two-photon fluorescence and IVIS imaging in the stomach. Balb/c female mice were randomly divided into three groups (SiMP, PDA MC, micromotor, n = 3). After that, 300 μL solution of FITC-labelled SiMP, PDA MC and micromotors were orally administered into the stomach of mice by using plastic feeding tubes (20 gauge × 30 mm). At 3 h post-administration, the mice were sacrificed, and their intact stomachs were excised and cut open through the great curvature of stomach to observe the wall. Then, the tissues were rinsed with PBS (pH 4.5), flattened, and visualized with a two-photon microscope (FV1000, Olympus, Japan). The two-photon fluorescence signal of FITC were observed with an excitation wavelength of 800 nm. The images were collected as Z-stacks (xyz, 400 Hz) at 512 × 512 pixels and analyzed with LAS AF Lite 2.6.1 of Leica. After intraoral injection of the samples into the stomach (3 h, 24 h and 3 d), the intact stomachs were excised from sacrificed mice for IVIS imaging with an IVIS Spectrum *in vivo* Imaging System (PerkinElmer, UK). *In vivo* experiments were conducted according to the institutional ethical protocols of POSTECH for animals (POSTECH-2018-0091**).**

Histological analysis. After intraoral injection of the samples into the stomach, the GI tract was excised from sacrificed mice and fixed in carnoy's solution for 12 h. The fixed GI tracts were embedded in paraffin blocks and 4-μm-thick sections were made for H&E staining. The stained sections were observed by optical microscopy (TCS SP5, Leica, Germany).

Statistical analysis. Data are expressed as means ± standard deviation (SD) from several separate experiments. All experiments were performed triplicate and 20 micromotors were measured for each group. The values for **$P < 0.01$ was considered statistically significant.

3. Results and discussions

Urease-powered micromotor was prepared by three fabrication steps (Fig. 1). First, dopamine molecules were polymerized onto the surface of silica microparticle (PDA@SiMP) in Tris-HCl buffer (pH 8.5). After that, silica core was removed by hydrofluoride (HF) solution to obtain a hollow polydopamine microcapsule (PDA MC). Then, ureases were immobilized onto the PDA MC by the reaction between amine group of an enzyme and the catechol group of PDA via a Schiff base reaction. Each step was checked by dynamic light scattering (DLS) (Fig. S1A). The hydrodynamic size of PDA@SiMP was increased after PDA coating. After silica core removal, the particle size of PDA MC was decreased to *ca.* 1 μm possibly due to the folds and creases of the hollow structure. After urease functionalization, the size of the micromotor was increased again, indicating the immobilization of urease onto the surface of PDA MC.

The characteristic morphology of micromotors was analyzed by high resolution - transmission electron microscopy (HR-TEM) (Fig. 2A). The micromotors were hollow capsules with a size of *ca.* 1 μm in accordance with the DLS data. Especially, with only very thin PDA shell, the propulsion of micromotors was very effective due to the light weight. Electron energy loss spectroscopy (EELS) revealed the components of micromotor including carbon, nitrogen, oxygen and sulfur (Fig. 2B). Remarkably, sulfur not in PDA but in urease was detected, indicating
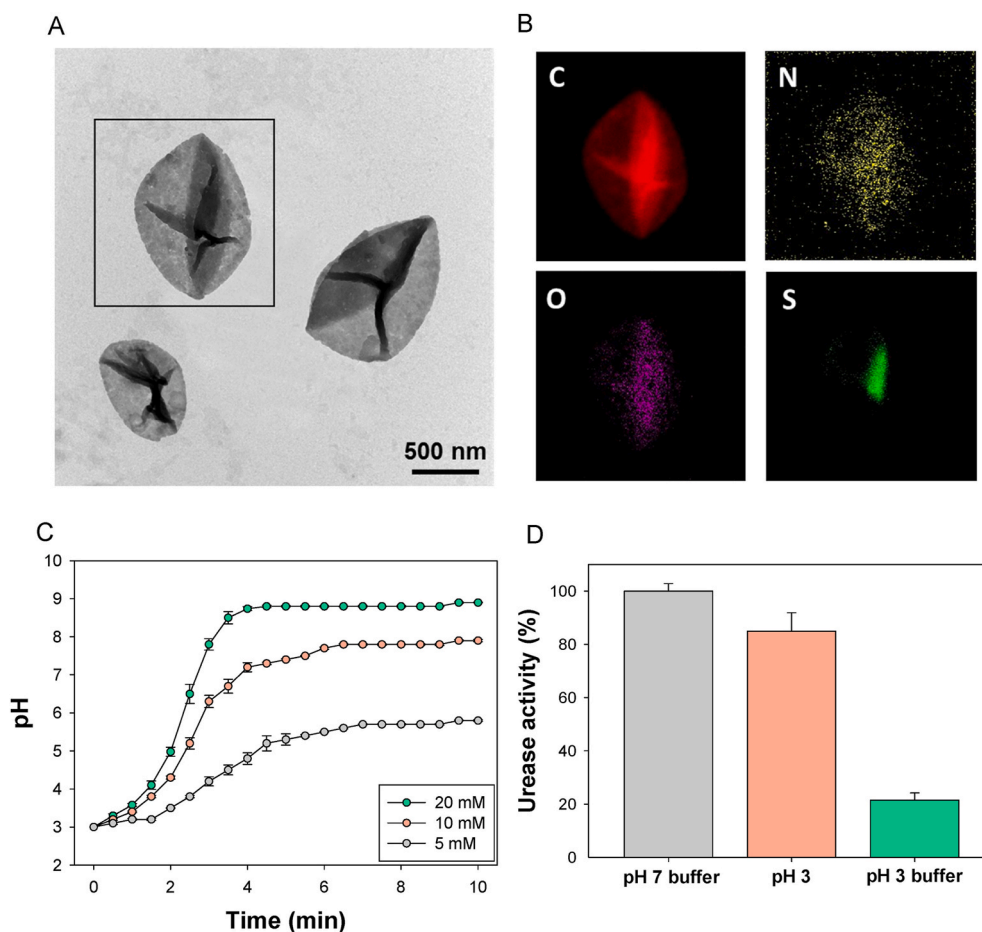
Fig. 2. (A) HR-TEM image of micromotors and (B) the corresponding EELS mapping of C in red, N in yellow, O in purple and S in green. (C) The pH increase of micromotor solution in the presence of urea (5, 10 and 20 mM). (D) The urease activity of micromotors in pH 3 and 7 buffer solutions, and pH 3 distiled ionic water.

successful functionalization of urease onto the surface of PDA MC. The sequential steps for the functionalization of PDA and the immobilization of urease were analyzed by FT-IR (Fig. S1B). The SiMP showed Si–O rocking vibration, Si–O bond stretching and strong Si–O–Si asymmetric stretching vibration peaks at 795, 950 and 1056 cm^{-1}, respectively. After coating with PDA, characteristic bonding peaks of PDA were observed at 1238, 1508 and 1620 cm^{-1}, corresponding to the C–O, C=C aromatic ring band and the vibration peak of N–H, respectively. After removing the SiO$_2$ core and grafting the urease, strong absorption peaks of SiO$_2$ disappeared and several characteristic peaks of urease appeared in the range of 1000–1650 cm^{-1}. Specifically, amide I band at 1643 cm^{-1} corresponded to the C=O stretching vibration of peptide linkages in the protein backbone. The amide II band at 1518 cm^{-1} is due to the combination of N–H bending and C–N stretching. This peak is also indicative of the formation of Schiff's base by the reaction between amine group of urease and catechol group of dopamine. The peak at 1084 cm^{-1} corresponded to sulfide group of urease.

After characterization of micromotors, we investigated the activity of immobilized urease by the addition of urea. The amount of urease on the surface of PDA MCs appeared to be 1.2 mg/mL according to the quantification by the BCA protein assay. In the stomach, urea is present in the range from 1 to 20 mM with a pH range from 3 to 7 in the mucus layer [32,33]. In accordance, we added the urea at a concentration of 5, 10 and 20 mM into the micromotor solution at an initial pH of 3. The urease-powered micromotor converted urea into ammonia and simultaneously increased pH (Fig. 2C). The pH was increased with increasing urea concentration from 5 to 20 mM. We also measured the zeta potential of PDA MC and the micromotor (Fig. S2). Since PDA has a zwitterionic property, the pH change can cause the zeta potential change

of PDA. Unlike PDA MC, the zeta potential of micromotors was changed from a positive charge (10 mV) to a negative charge (−33 mV) by the addition of urea. From the results, we could confirm that urease was successfully immobilized onto the surface of PDA MC and the urease efficiently increased the pH upon the addition of urea. Then, we assessed the activity of immobilized urease according to pH (Fig. 2D). In a buffer solution at pH 3, urease activity was only 20% of that at pH 7, because urease activity is optimal at pH 7.4 and gradually decreases with decreasing pH. Remarkably, in water at pH 3, the activity of immobilized urease was significantly increased to 83% due to the pH increase during the analysis (Fig. 2C). Fig. S3 shows the amount of ammonia generated by the decomposition of urea in PBS (pH 7.4) and gastric fluid (pH 3). The ammonia generation in gastric fluid was comparable to that in PBS (85.9%), in accordance with Fig. 2C. The results revealed that the immobilized urease could efficiently convert urea even in the acidic condition of stomach.

The urease-powered micromotor is propelled by converting urea into ammonia and carbon dioxide as follows: (NH$_2$)$_2$CO + H$_2$O → CO$_2$ + 2NH$_3$. At a low Reynolds number, inducing geometrical asymmetry of synthetic motors is an important requirement for self-propulsion. However, recent studies demonstrated that the molecularly unbalanced distribution of enzymes could also generate propulsion power efficiently via bio-catalytic conversion [34,35]. The motion analysis of urease-powered micromotors was investigated according to the urea concentration of 0, 5, 10 and 20 mM. We tracked the micromotors for 10 s using the optical tracking method, which recorded 35 frames per sec (Fig. 3A). The mean-squared displacement (MSD) was calculated from the trajectories (Fig. 3B). The micromotors were randomly diffused by Brownian motion without any directionality in the absence of the urea.
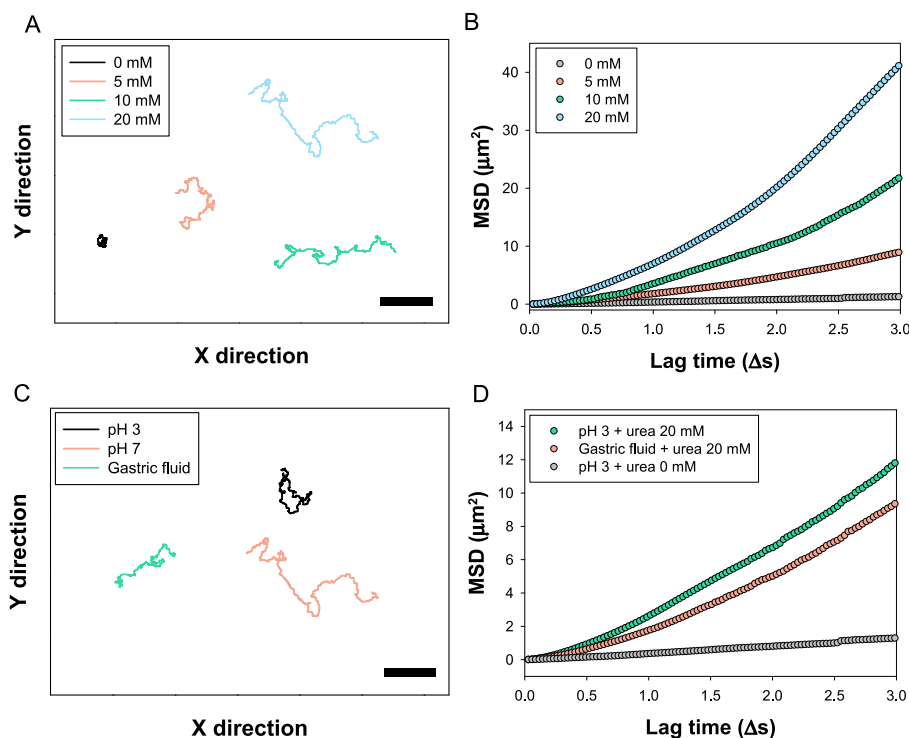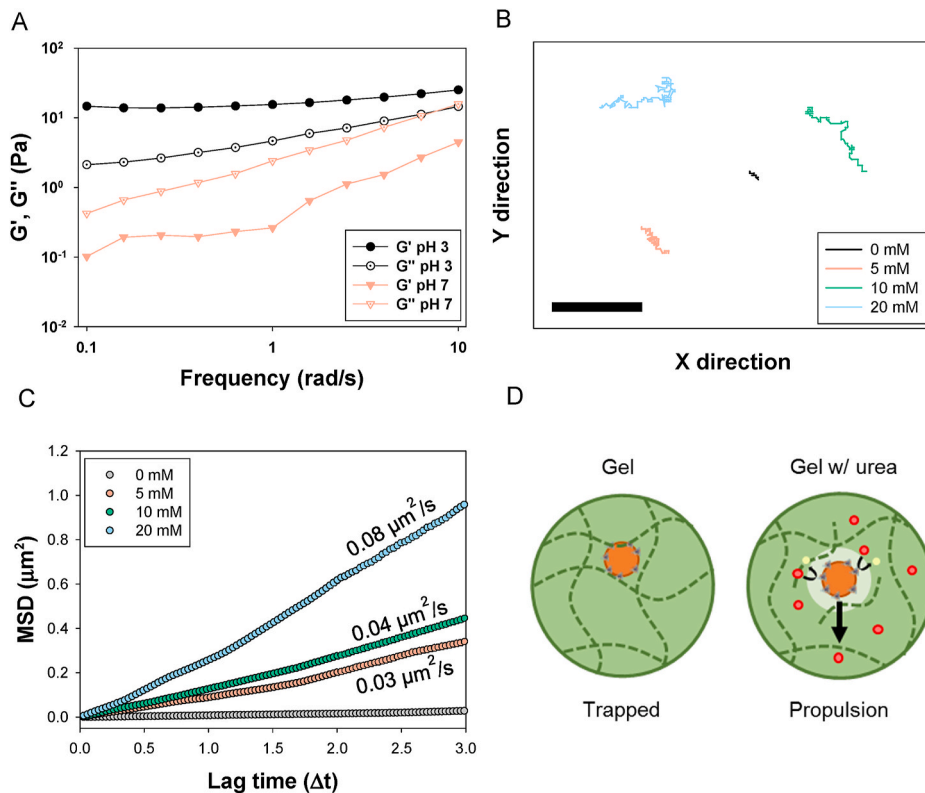
Fig. 3. (A) The trajectories of representative micromotors for 10 s and (B) the corresponding mean square displacement (MSD) with increasing lag time at 0, 5, 10 and 20 mM. (C) The trajectories of representative micromotors for 10 s at pH 3, 7 and gastric fluid and (D) the MSD with increasing lag time at pH 3 (w/o urea), pH 3 (w/urea) and gastric fluid (w/urea). The MSD was analyzed by the X and Y coordinates tracking of 20 particles. The velocity was calculated by fitting the MSD data to the following equation: $(v \times \Delta t)^2 + 4 \times D_e \times \Delta t$. (scale bar = 5 μm).

In addition, MSD curve was increased linearly as typically observed in the Brownian motion. Meanwhile, the micromotors moved fast and showed directionality at the urea concentration of 5, 10 and 20 mM (Movies S1, S2 and S3). For these cases, the corresponding MSD was increased non-linearly at a velocity of 0.78, 1.31 and 1.9 μm/s, respectively. We also assessed the pH and ionic strength effect on the movement of micromotor (Fig. 3C, Movies S4 and S5). As reported elsewhere [36], self-diffusiophoresis propulsion by enzyme can be affected by the pH and ionic strength. The movement of micromotors was more suppressed at pH 3 and in gastric fluid than that at pH 7. However, they still showed efficient movement at a velocity of 1.13 and 0.63 μm/s, respectively. Despite the harsh condition at the low pH and

Fig. 4. (A) The viscoelastic properties of mucin gels at different pH conditions. A mucin gel exhibits a clear sol-gel transition between pH 3 and pH 7. Closed symbols denote the storage modulus G′, and open symbols denote the loss modulus G′′. (B) The trajectories of representative micromotors in the mucin gel for 40 s and (C) the corresponding MSD with increasing lag time in 0, 5, 10 and 20 mM urea. (D) Schematic illustration for the penetration mechanism of micromotor in mucin gel by the local gel-sol transition. MSD was analyzed by the X and Y coordinates tracking of 20 particles. The diffusion coefficient was calculated by fitting the MSD data to the following equation: $4 \times D_e \times \Delta t$ (scale bar = 3 μm).

ionic media, the micromotor could efficiently propel in the gastric fluid.

Supplementary data related to this article can be found at https://doi.org/10.1016/j.bioactmat.2021.08.004.

In order to confirm the penetration of PDA micromotor through the mucus layer, we made a mucin gel as an *in vitro* model of mucus layer. As shown in Fig. 4A, storage modulus (G′) is bigger than loss modulus (G″) at the whole range of frequency at pH 3, indicating the gel state. In contrast, G″ is bigger than G′ at pH 7, indicating the sol state. This gel showed the gel-sol transition behavior depending on pH, which is the typical characteristic of *in vivo* mucus layer with comparable value of modulus to *in vivo* mucus layer [19,37]. We evaluated the motion of micromotors in the mucin gel for 40 s (Fig. 4B). At pH 3 without urea, the micromotors could hardly move and even did not show any Brownian motion because of the trapping in the polymer networks (Fig. 4C and Movie S6). However, at pH 3 with urea (5, 10 and 20 mM), the micromotors showed enhanced diffusion with a diffusion coefficient of 0.03, 0.04 and 0.08 μm^2/s, respectively (Movie S7, S8 and S9). The micromotors were able to induce the local gel-sol transition of mucin gel and penetrate the mucin by the propulsion (Fig. 4D). Because of relatively slow and mild penetration mechanism in comparison with metal-mediated redox reaction, the micromotors might not cause any significant damage to the stomach tissues.

Supplementary data related to this article can be found at https://doi.org/10.1016/j.bioactmat.2021.08.004.

On the basis of *in vitro* data, we investigated *in vivo* fate of micromotors after oral delivery. Three groups of SiMP, PDA MC and micromotor were visualized by fluorescence imaging after tagging with FITC (Fig. S4). Balb/c mice were treated by the oral administration of the samples (300 μL) using oral feeding tubes. We obtained IVIS images and quantified the fluorescent intensity of whole stomach for 3 days (Fig. 5A and B). In a stomach, mucus layer is composed of two layers, where an outer layer is loose and cleared easily, and an inner mucus layer is firmly attached to the epithelium and slowly cleared. Thus, the penetration up to the inner mucus layer is necessary for the enhanced retention in the stomach. At 3 h post-injection, PDA MC and micromotor groups showed strong fluorescence intensity in the stomach. Since PDA has mucoadhesive property, PDA MC and micromotor groups could be retained, adhering to the mucus layer even after stomach clearance time of 3 h. While most of PDA MC were cleared in a day, the micromotors showed the better retention behavior. We confirmed that PDA MC were just attached to the outer mucus layer, but the micromotors deeply penetrated up to the inner mucus. In addition, the tendency of clearance in intestine is similar with that of stomach (Fig. 5C). The micromotors were slowly removed and totally cleared from the GI tract within 3 days, indicating that this urease-powered micromotor system might be a feasible drug delivery carrier for the treatment of stomach diseases.

To assess the deep penetration of micromotors into the stomach, mice were sacrificed and stomachs were excised at 3 h post-injection.
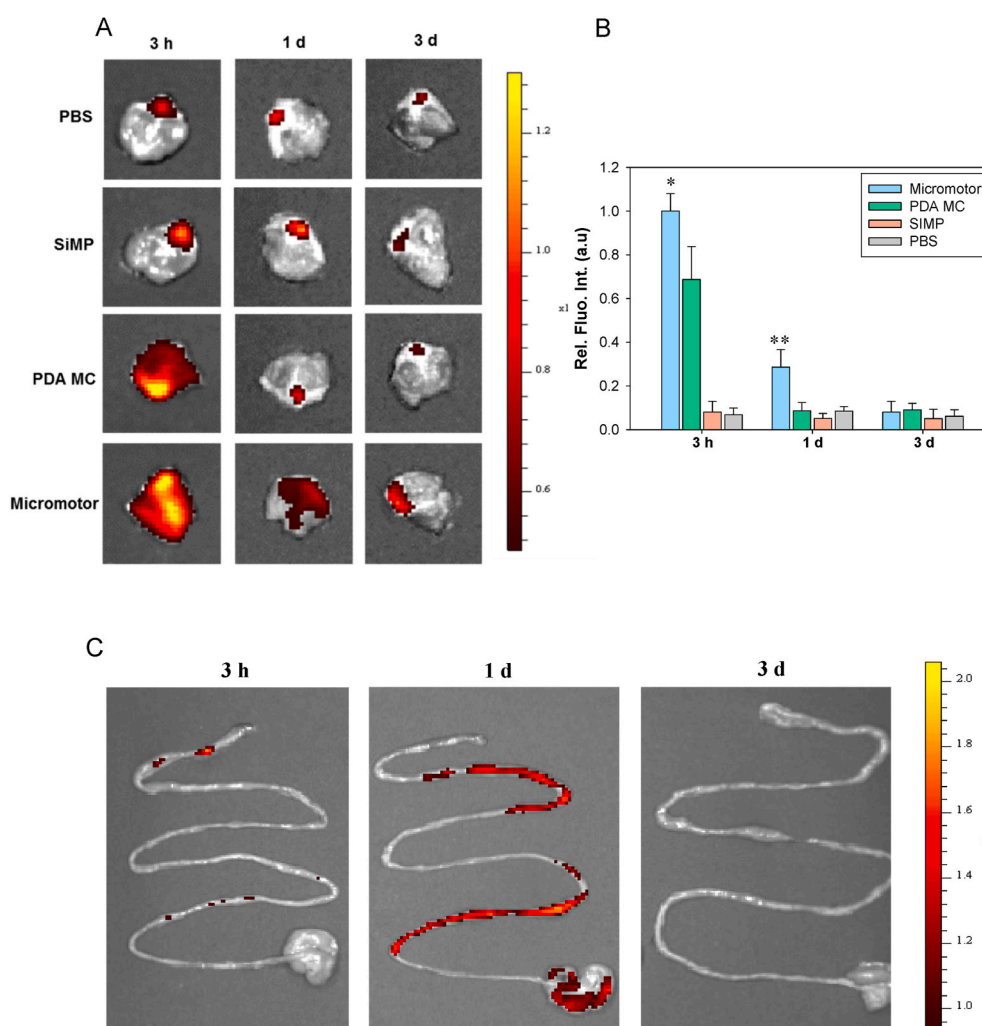

Fig. 5. (A) IVIS images of intact stomach at 3 h, 1 d and 3 d post-oral injection of PBS, SiMP, PDA MC and micromotors and (B) the corresponding quentified fluorescence intensity at each time point (n = 3). (C) IVIS images of intestinal tract at 3 h, 1 d and 3 d post-oral administration of micromotors. (*$P \leq 0.05$, **$P \leq 0.01$, Micromotor *vs* PDA MC).

The stomachs were cut open through the greater curvature of stomach to observe the stomach wall by two-photon microscopy. As shown in maximum projection images (Fig. 6A), only week fluorescence was observed on the stomach wall in the case of SiMP group. In contrast, strong fluorescence was observed on the stomach wall in the cases of PDA MC due to the muco-adhesive property of PDA. Remarkably, considerable fluorescence of micromotors could be observed due to the deep penetration through the mucus layer. The penetration depth of micromotors was clearly confirmed by the Z-stacked fluorescence images (second row of Figs. 6A and S5). As expected, the micromotor group penetrated deeper than other groups through the stomach wall. Then, we sectioned the tissues and stained with Hematoxylin and Eosin (H&E) for further confirmation of penetration through the mucus layer. As shown in Fig. 6B, mucus layer was clearly observed with a thickness of *ca.* 50–70 μm (dotted line in the PBS group). We could observe the PDA MC and micromotors penetrated into the mucus layer. Especially, micromotors showed deep penetration and prolonged retention in the mucus layer in accordance with Fig. 5A.

After investigating the enhanced penetration of micromotors, histological analysis of the GI tract tissues was performed with H&E staining to assess the tissue toxicity (Fig. 7). PBS and micromotors were orally administered into mice, and the tissues from GI tract were excised from sacrificed mice and fixed at 3 days post-injection for H&E staining. We obtained tissues from 4 parts of GI tract including stomach, duodenum, ileum and colon. There was no significant histological difference between PBS and the micromotor treated tissues with no significant lesion in both GI tract tissues. More specifically, the size and number of crypt and villus were not different between two groups and lymphocytic infiltration into the mucosa and submucosa were not observed in both groups, indicating no sign of gastric inflammation. From the histological analysis, we could confirm that the micromotors were cleared without causing any tissue toxicity and the feasibility for further clinical applications.

Finally, for potential use of the micromotor for treating stomach diseases, we investigated the biodegradability of micromotors (Fig. S6). The degradation profile of micromotors was qualitatively investigated by measuring absorbance and TEM at pH 3 and in the presence of H_2O_2 (10 mM) as the typical *in vivo* condition of oxidative stress at the diseased tissue [38]. In the oxidative condition, absorbance and color of micromotor solution slowly faded for 14 days. In addition, TEM images also showed the biodegradation of micromotors after 14 days. From the degradation data, we confirmed that the micromotors were rapidly degraded in oxidative condition, demonstrating feasibility of potential use of treating stomach diseases.
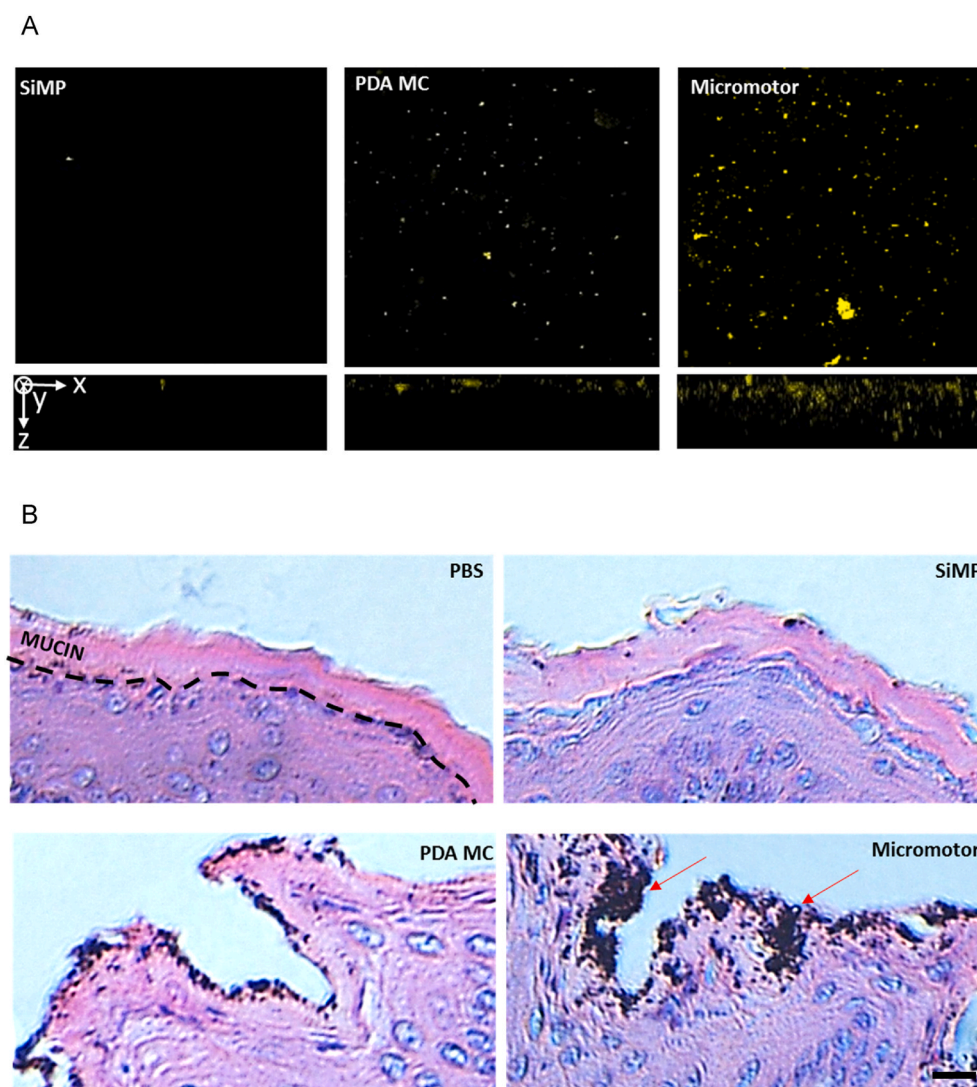
Fig. 6. (A) Two-photon microscopic images of stomach wall (first row) and the corresponding Z-stack images (second row) at 3 h post-oral injection of FITC-labelled SiMP, PDA MC and micromotors (scale bar = 100 μm). (B) H&E staining of stomach wall at 3 h post-oral injection of SiMP, PDA MC and micromotors. Red arrows indicate micromotors (scale bar = 50 μm).

Control   **Micromotor**
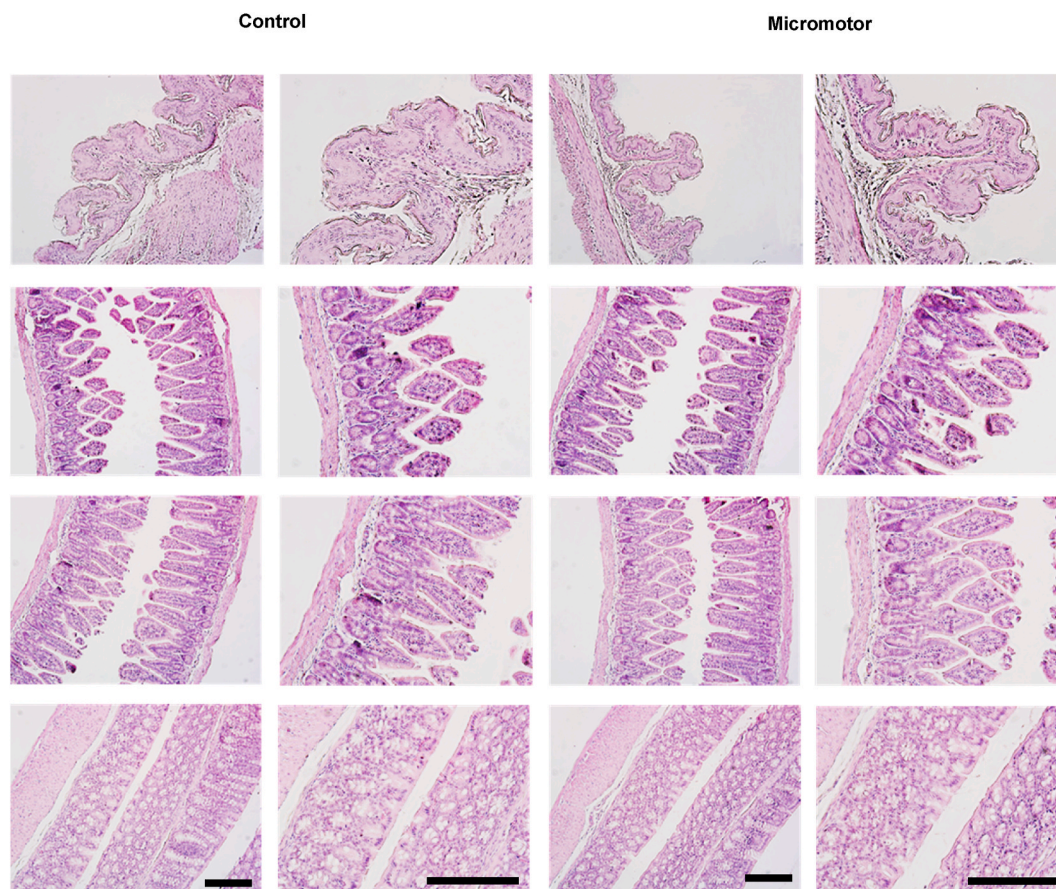

Fig. 7. Histological analysis with H&E staining of stomach (first row), duodenum (second row), ileum (thrird row) and colon (last row) at 3 d post-injection of PBS and micromotors (scale bar = 200 μm).

4. Conclusions

In conclusion, we successfully developed urease-powered PDA micromotors as an active oral delivery carrier in the stomach. HR-TEM, EELS mapping, DLS, zeta-potential analysis and urease activity test showed the successful fabrication of urease-functionalized micromotors. *In vitro* movement analysis in various condition (pH 3, gastric fluid and mucin gel) confirmed the feasibility of urease-powered micromotors for the applications in the stomach. After oral administration, the micromotors showed significantly improved penetration and prolonged retention in the stomach for a day. In addition, the micromotors appeared to be cleared within 3 days without causing any GI tract toxicity. Taken together, we could confirm the feasibility of micromotors for further applications to various stomach diseases. These clearable polydopamine micromotors would be harnessed to encapsulate various anticancer drugs such as doxorubicin via π-π interactions with catechol group of polydopamine for stomach cancer therapy.

CRediT authorship contribution statement

Hyunsik Choi: Conceptualization, Methodology, Validation, Investigation, Formal analysis, Writing – original draft, Writing – review & editing. **Sang Hoon Jeong:** Methodology, Validation, Investigation. **Tae Yeon Kim:** Methodology, Validation, Investigation. **Jeeyoon Yi:** Methodology, Validation, Investigation. **Sei Kwang Hahn:** Supervision, Project administration, Funding acquisition.

Declaration of competing interest

The authors declare that they have no known competing financial interests or personal relationships that could have appeared to influence the work reported in this paper.

Appendix A. Supplementary data

Supplementary data to this article can be found online at https://doi.org/10.1016/j.bioactmat.2021.08.004.

References

[1] M.E.V. Johansson, H. Sjövall, G.C. Hansson, The gastrointestinal mucus system in health and disease, Nat. Rev. Gastroenterol. Hepatol. 10 (2013) 352–361.

[2] R.A. Cone, Barrier properties of mucus, Adv. Drug Deliv. Rev. 61 (2009) 75–85.

[3] M.A. McGuckin, S.K. Lindén, P. Sutton, T.H. Florin, Mucin dynamics and enteric pathogens, Nat. Rev. Microbiol. 9 (2011) 265–278.

[4] L.M. Ensign, R. Cone, J. Hanes, Oral drug delivery with polymeric nanoparticles: the gastrointestinal mucus barriers, Adv. Drug Deliv. Rev. 64 (2012) 557–570.

[5] C. Gao, Y. Wang, Z. Ye, Z. Lin, X. Ma, Q. He, Biomedical micro-/nanomotors: from overcoming biological barriers to in vivo imaging, Adv. Mater. (2020) 2000512.

[6] M. Luo, Y. Feng, T. Wang, J. Guan, Micro-/Nanorobots at work in active drug delivery, Adv. Funct. Mater. 28 (2018) 1706100.

[7] E. Karshalev, Y. Zhang, B. Esteban-Fernández de Ávila, M. Chen, R. Mundaca-Uribe, F. Zhang, B. Nguyen, Y. Tong, R. Fang, L. Zhang, J. Wang, Micromotors for

active delivery of minerals toward the treatment of iron deficiency anemia, Nano Lett. 19 (2019) 7816–7826.

[8] J. Li, S. Thamphiwatana, W. Liu, B. Esteban-Fernández de Ávila, P. Angsantikul, E. Sandraz, J. Wang, T. Xu, F. Soto, V. Ramez, X. Wang, W. Gao, L. Zhang, J. Wang, Enteric micromotor can selectively position and spontaneously propel in the gastrointestinal tract, ACS Nano 10 (2016) 9536–9542.

[9] B. Esteban-Fernández de Ávila, P. Angsantikul, J. Li, M.A. Lopez-Ramirez, D. E. Ramírez-Herrera, S. Thamphiwatana, C. Chen, J. Delezuk, R. Samakapiruk, V. Ramez, M. Obonyo, L. Zhang, J. Wang, Micromotor-enabled active drug delivery for in vivo treatment of stomach infection, Nat. Commun. 8 (2017) 272.

[10] B. Esteban-Fernández de Ávila, M.A. Lopez-Ramirez, R. Mundaca-Uribe, X. Wei, D. E. Ramírez-Herrera, E. Karshalev, B. Nguyen, R.H. Fang, L. Zhang, J. Wang, Multicompartment tubular micromotors toward enhanced localized active delivery, Adv. Mater. 32 (2020), e2000091.

[11] Z. Wu, L. Li, Y. Yang, P. Hu, Y. Li, S.Y. Yang, L.V. Wang, W. Gao, A microrobotic system guided by photoacoustic computed tomography for targeted navigation in intestines in vivo, Sci. Robot. 4 (2019), eaax0613.

[12] W. Gao, R. Dong, S. Thamphiwatana, J. Li, W. Gao, L. Zhang, J. Wang, Artificial micromotors in the mouse's stomach: a step toward in vivo use of synthetic motors, ACS Nano 9 (2015) 117–123.

[13] J. Li, P. Angsantikul, W. Liu, B.E.-F. deÁvila, S. Thamphiwatana, M. Xu, E. Sandraz, X. Wang, J. Delezuk, W. Gao, L. Zhang, J. Wang, Micromotors spontaneously neutralize gastric acid for pH-responsive payload release, Angew. Chem. Int. Ed. 56 (2017) 2156–2161.

[14] H. Choi, S.H. Cho, S.K. Hahn, Urease-powered polydopamine nanomotors for intravesical therapy of bladder diseases, ACS Nano 14 (2020) 6683–6692.

[15] R. Cheng, W. Huang, L. Huang, B. Yang, L. Mao, K. Jin, Q. ZhuGe, Y. Zhao, Acceleration of tissue plasminogen activator-mediated thrombolysis by magnetically powered nanomotors, ACS Nano 8 (2014) 7746–7754.

[16] M. Wan, Q. Wang, R. Wang, R. Wu, T. Li, D. Fang, Y. Huang, Y. Yu, L. Fang, X. Wang, Y. Zhang, Z. Miao, B. Zhao, F. Wang, C. Mao, Q. Jiang, X. Xu, D. Shi, Platelet-derived porous nanomotor for thrombus therapy, Sci. Adv. 6 (2020) eaaz9014.

[17] W. He, J. Frueh, N. Hu, L. Liu, M. Gai, Q. He, Guidable thermophoretic janus micromotors containing gold nanocolorifiers for infrared laser assisted tissue welding, Adv. Sci. 3 (2016) 1600206.

[18] O. Felfoul, M. Mohammadi, S. Taherkhani, D. de Lanauze, Y.Z. Xu, D. Loghin, S. Essa, S. Jancik, D. Houle, M. Lafleur, L. Gaboury, M. Tabrizian, N. Kaou, M. Atkin, T. Vuong, G. Batist, N. Beauchemin, D. Radzioch, S. Martel, Magneto-aerotactic bacteria deliver drug-containing nanoliposomes to tumour hypoxic regions, Nat. Nanotechnol. 11 (2016) 941–947.

[19] D. Walker, B.T. Käsdorf, H.-H. Jeong, O. Lieleg, P. Fischer, Enzymatically active biomimetic micropropellers for the penetration of mucin gels, Sci. Adv. 1 (2015), e1500501.

[20] P.S. Schattling, M.A. Ramos-Docampo, V. Salgueiriño, B. Städler, Double-fueled janus swimmers with magnetotactic behavior, ACS Nano 11 (4) (2017) 3973–3983.

[21] L.K. Abdelmohsen, M. Nijemeisland, G.M. Pawar, G.J.A. Janssen, R.J. Nolte, J. C. van Hest, D.A. Wilson, Dynamic loading and unloading of proteins in polymeric stomatocytes: formation of an enzyme-loaded supramolecular nanomotor, ACS Nano 10 (2) (2016) 2652–2660.

[22] X. Ma, X. Wang, K. Hahn, S. Sánchez, Motion control of urea-powered biocompatible hollow microcapsules, ACS Nano 3 (2016) 3597–3605.

[23] A.C. Hortelao, C. Simó, M. Guix, S. Guallar-Garrido, E. Julián, D. Vilela, L. Rejc, P. Ramos-Cabrer, U. Cossío, V. Gómez-Vallejo, T. Patiño, J. Llop, S. Sánchez,

[24] Z. Wang, K. Wang, Y. Zhang, Y. Jiang, X. Lu, L. Fang, D. Gan, C. Lv, H. Zhang, S. Qu, Protein-affinitive polydopamine nanoparticles as an efficient surface modification strategy for versatile porous scaffolds enhancing tissue regeneration, Part. Part. Syst. Char. 33 (2016) 89–100.

[25] C. Rodriguez-Emmenegger, C.M. Preuss, B. Yameen, O. PopGeorgievski, M. Bachmann, J.O. Mueller, M. Bruns, A.S. Goldmann, M. Bastmeyer, C. Barner-Kowollik, Controlled cell adhesion on poly(dopamine) interfaces photopatterned with non-fouling brushes, Adv. Mater. 25 (2013) 6123–6127.

[26] K. Yang, J.S. Lee, J. Kim, Y.B. Lee, H. Shin, S.H. Um, J.B. Kim, K.I. Park, H. Lee, S. W. Cho, Polydopamine-mediated surface modification of scaffold materials for human neural stem cell engineering, Biomaterials 33 (2012) 6952–6964.

[27] S. Sunoqrot, L. Hasan, A. Alsadi, R. Hamed, O. Tarawneh, Interactions of mussel-inspired polymeric nanoparticles with gastric mucin: implications for gastro-retentive drug delivery, Colloids Surf. B Biointerfaces 156 (2017) 1–8.

[28] J.P. Celli, B.S. Turner, N.H. Afdhal, S. Keates, I. Ghiran, C.P. Kelly, R.H. Ewoldt, G. H. McKinley, P. So, S. Erramilli, R. Bansil, Helicobacter pylori moves through mucus by reducing mucin viscoelasticity, Proc. Natl. Acad. Sci. Unit. States Am. 106 (2009) 14321–14326.

[29] X. Cao, R. Bansil, K.R. Bhaskar, B.S. Turner, J.T. LaMont, N. Niu, N.H. Afdhal, pH-dependent conformational change of gastric mucin leads to sol-gel transition, Biophys. J. 76 (1999) 1250–1258.

[30] B. Yu, D.A. Wang, Q. Ye, F. Zhou, W. Liu, Robust polydopamine nano/microcapsules and their loading and release behavior, Chem. Commun. (2009) 6789–6791.

[31] J. Weng, S. Zhao, Z. Li, K.B. Ricardo, F. Zhou, H. Kim, H. Liu, Raman enhancement and photo-bleaching of organic dyes in the presence of chemical vapor deposition-grown graphene, Nanomaterials 7 (2017) 337.

[32] H. Kim, C. Park, W.I. Jang, K.H. Lee, S.O. Kwon, S.S. Robey-Cafferty, J.Y. Ro, Y. B. Lee, The gastric juice urea and ammonia levels in patients with Campylobacter pylori, Am. J. Clin. Pathol. 94 (1990) 187–191.

[33] S. Schreiber, M. Konradt, C. Groll, P. Scheid, G. Hanauer, H.-O. Werling, C. Josenhans, S. Suerbaum, The spatial orientation of Helicobacter pylori in the gastric mucus, Proc. Natl. Acad. Sci. Unit. States Am. 101 (2004) 5024–5029.

[34] A.C. Hortelão, R. Carrascosa, N. Murillo-Cremaes, T. Patiño, S. Sánchez, Targeting 3D bladder cancer spheroids with urease-powered nanomotors, ACS Nano 13 (2019) 429–439.

[35] T. Patino, N. Feiner-Gracia, X. Arque, A. Miguel-Lopez, A. Jannasch, T. Stumpp, E. Schaffer, L. Albertazzi, S. Sanchez, *I*nfluence of enzyme quantity and distribution on the self-propulsion of non-janus urease-powered micromotors, J. Am. Chem. Soc. 1*40* (2018) 7896–7903.

[36] A. Brown, W. Poon, Ionic effects in self-propelled Pt-coated janus swimmers, Soft Matter 10 (2014) 4016–4027.

[37] J.P. Celli, B.S. Turner, N.H. Afdhal, R.H. Ewoldt, G.H. McKinley, R. Bansil, S. Erramilli, Rheology of gastric mucin exhibits a pH-dependent sol-gel transition, Biomacromolecules 8 (2007) 1580–1586.

[38] M. Battaglini, A. Marino, A. Carmignani, C. Tapeinos, V. Cauda, A. Ancona, N. Garino, V. Vighetto, G.L. Rosa, E. Sinibaldi, G. Ciofani, Polydopamine nanoparticles as an organic and biodegradable multitasking tool for neuroprotection and remote neuronal stimulation, ACS Appl. Mater. Interfaces 12 (2020) 35782–35798.